

Microscopic mechanism for the shear-thickening of non-Brownian suspensions

Nicolas Fernandez,¹ Roman Mani,² David Rinaldi,³ Dirk Kadau,² Martin Mosquet,³ H el ene Lombois-Burger,³ Juliette Cayer-Barrioz,⁴ Hans J. Herrmann,² Nicholas D. Spencer,¹ and Lucio Isa^{1,*}

¹Laboratory for Surface Science and Technology, Department of Materials, ETH Zurich, Switzerland

²Computational Physics for Engineering Materials, Department of Civil, Environmental and Geomatic Engineering, ETH Zurich, Switzerland

³Lafarge LCR, Saint Quentin-Fallavier, France

⁴Laboratoire de Tribologie et Dynamique des Syst emes - UMR 5513 CNRS,  Ecole Centrale de Lyon, France

We propose a simple model, supported by contact-dynamics simulations as well as rheology and friction measurements, that links the transition from continuous to discontinuous shear-thickening in dense granular pastes to distinct lubrication regimes in the particle contacts. We identify a local Sommerfeld number that determines the transition from Newtonian to shear-thickening flows, and then show that the suspension's volume fraction and the boundary lubrication friction coefficient control the nature of the shear-thickening transition, both in simulations and experiments.

Flow non-linearities attract fundamental interest and have major consequences in a host of practical applications [1, 2]. In particular, shear-thickening (ST), a viscosity increase from a constant value (Newtonian flow-Nw) upon increasing shear stress (or rate) at high volume fraction ϕ , can lead to large-scale processing problems of dense pastes, including cement slurries [3]. Several approaches have been proposed to describe the microscopic origin of shear-thickening [4–7]. The most common explanation invokes the formation of "hydroclusters", which are responsible for the observed continuous viscosity increase [6, 8, 9] and which have been observed for Brownian suspensions of moderate volume fractions [10, 11]. However, this description no longer holds for bigger particles and denser pastes, where contact networks can develop and transmit positive normal stresses [12]. Moreover, the link between hydroclusters and CST for non-Brownian suspensions is still a matter of debate [13]. Additionally, dense, non-Brownian suspensions can also show sudden viscosity divergence under flow [14–17] with catastrophic effects, such as pumping failures. In contrast to a continuous viscosity increase at any applied rate, defined as continuous shear-thickening (CST), the appearance of an upper limit of the shear rate defines discontinuous shear-thickening (DST). This CST to DST transition is observed when the volume fraction of the flowing suspension is increased above a critical value, which depends on the system properties, e.g. polydispersity or shape, and on the flow geometry [3, 18]. An explanation for its microscopic origin is still lacking [19]. Moreover, experiments have demonstrated that the features of the viscosity increase (slope, critical stress) can be controlled by tuning particle surface properties such as roughness [20] and/or by adsorbing polymers [21, 22]. These findings suggest that inter-particle contacts play a crucial role in the macroscopic flow at high volume fractions. A more precise description of these contacts is therefore essential to interpret the rheological behavior.

In this paper, we present a unified theoretical framework, supported by both numerical simulations and ex-

perimental data, which describes the three flow regimes of rough, frictional, non-Brownian particle suspensions (Nw,CST,DST) and links the Nw-ST (in terms of shear) and the CST-DST transitions (in terms of volume fraction) to the local friction. Our microscopic particle-contact based description, as opposed to macroscopic scaling, explains both the occurrence of DST and recovers Bagnold's analysis [5] for CST, respectively above and below a critical volume fraction.

The lubricated contact between two solid surfaces has been widely studied in the past [23]. It is now commonly accepted that different lubrication regimes occur as a function of a characteristic number, the Sommerfeld number s . For two identical spheres, $s = \eta_f v R_p / N$, where η_f is the fluid viscosity, v is the sliding speed between the two solid surfaces, R_p is the radius of the spheres and N is the normal load. At high s ("hydrodynamic regime"-HD), a fluid film fully separates the two sliding surfaces and the friction coefficient μ depends on s . For low s , below a critical value s_c , the lubrication film breaks down and contacts between the microscopic asperities on each surface support most of the load. This "boundary lubrication" regime (BL) exhibits friction coefficients that only very weakly depend on s . For intermediate values of s the system is in a "mixed regime", where the sharpness of the transition depends on the system properties (e.g. contact roughness, rheology of the fluid. See Fig.1a) [23].

Both experiments and models show that Nw flow is stable below a critical shear rate $\dot{\gamma}_c$ where the contacts between particles are HD lubricated. On the other hand, a particle-contact-dominated flow requires, by definition, that $s < s_c$ and it is equivalent to a dense dry granular flow (i.e. no suspending fluid lubrication effects). Dense granular flows follow a quadratic scaling of the normal and shear stress P and τ with the shear rate $\dot{\gamma}$

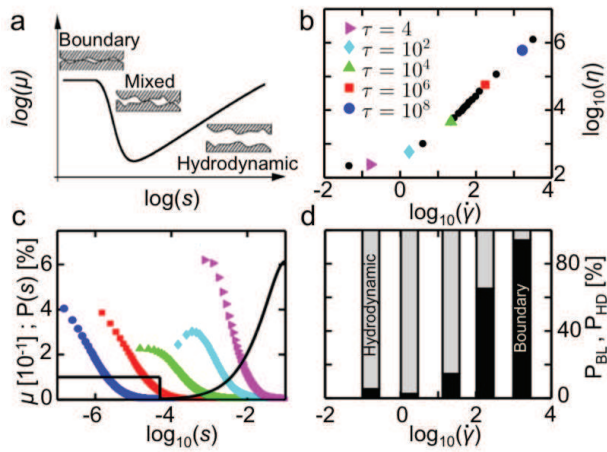


FIG. 1. (color online) a) Schematic Stribeck curve. Evolution of the friction coefficient, μ , versus the Sommerfeld number, s , for a lubricated contact. b) Apparent viscosity, η , versus the shear rate, $\dot{\gamma}$, from the numerical simulations. c) Numerical simulations friction law (black line) and probability distributions of s , $P(s)$, for all contacts at several shear stresses as defined in b. d) Frequencies of BL contacts, P_{BL} , and HD contacts, $P_{HD} = 1 - P_{BL}$, as a function of $\dot{\gamma}$ for the stresses defined in b. The simulations data in b-c-d have $\phi = 0.58$, $\mu_0 = 0.1$ and $s_c = 5 \times 10^{-5}$.

(Bagnold scaling) through a volume-fraction-dependent factor [5]; this implies that the apparent viscosity rises linearly with $\dot{\gamma}$ and that the system shear thickens continuously (see Fig.1b). This scaling can be expressed in terms of a dimensionless parameter, the inertial number $I = \dot{\gamma} R_p \sqrt{\frac{\rho_p}{P}}$, only depending on ϕ and μ for rigid particles with density ρ_p [24].

Given the definition of s , this leads to $s \propto \eta_f I^2 / \dot{\gamma} \rho_p R_p^2$. This Bagnold (CST) regime is possible as long as $\dot{\gamma}$ is larger than $\dot{\gamma}_c \propto \eta_f I^2 / s_c \rho_p R_p^2$, showing the link between $\dot{\gamma}_c$ and s_c when particle contacts dominate. This transition was partially proposed, with macroscopic arguments, by Bagnold [5, 25, 26]. Nevertheless, our microscopic analysis also accounts for volume fraction effects.

In our model, the existence of two lubrication mechanisms (boundary and hydrodynamic) implies two different jamming volume fractions ϕ_{max} , above which flow is not possible. If the system is hydrodynamically lubricated, the jamming volume fraction ϕ_{max}^{HD} is at random close packing ϕ_{RCP} , regardless of the boundary friction coefficient [27]. Conversely, when the system is in a boundary-lubricated Bagnold regime, the jamming volume fraction ϕ_{max}^{BL} decreases with μ [28, 29]. Both ϕ_{max}^{HD} and ϕ_{max}^{BL} are independent of $\dot{\gamma}$ for non-Brownian particles. It follows that $\phi_{RCP} = \phi_{max}^{HD} \geq \phi_{max}^{BL}(\mu)$. When $\phi \leq \phi_{max}^{BL} \leq \phi_{max}^{HD}$, the transition from hydrodynamic to boundary-dominated flow is possible and

the suspension exhibits CST, as reported above and predicted by Bagnold. When $\phi_{max}^{BL} < \phi \leq \phi_{max}^{HD}$, the transition to a Bagnold regime is forbidden, and the shear rate cannot exceed $\dot{\gamma}_c$: the system undergoes DST. As a consequence, ϕ_{max}^{BL} is the critical volume fraction for DST and therefore it can be tuned by changing the particle friction coefficient. Both numerical simulations and experiments fully and independently support our model.

In concentrated systems most of the dissipation arises from particles that are in, or close to, contact and not from Stokesian drag [25, 30]. This motivates using Contact Dynamics [31–35] to simulate dense suspensions of hard, spherical, frictional particles using a simplified Stribeck curve (no mixed regime) as friction law (see Fig.1c and Eq.1). Only one dissipative mechanism, either BL or HD, is taken into account in each contact. This constitutes the simplest physical description of a lubricated contact.

The boundary lubrication between two rough particles is described using Amontons-Coulomb friction, i.e. the coefficient of friction μ_0 being independent of the load, the speed and the apparent contact area [23].

In the HD regime, the hydrodynamic interactions between two neighboring particles are long-lived and can be described by standard, low-Reynolds-number fluid mechanics with a lubrication hypothesis [36], from which a friction coefficient can be calculated as a function of the Sommerfeld number $\mu = 2\pi s \ln(\frac{5}{6\pi s})$ (see Supplemental Material for full derivation). The lubrication hypothesis breaks down when the particles are too far apart (i.e. when s is large) and therefore we consider only a range of $\dot{\gamma}$ where s of almost all the contacts is smaller than a limit value, $s_{lim} = 10^{-1}$.

The friction law used for the simulations is then:

$$\mu(s) = \begin{cases} \mu_0 & \text{if } s < s_c \\ 2\pi s \ln(\frac{5}{6\pi s}) & \text{if } s_c < s < s_{lim} \end{cases} \quad (1)$$

In our Contact Dynamics simulations the normal forces are calculated based on perfect volume exclusion, using zero normal restitution coefficient, and we simulate stress-controlled (τ) simple shear between moving and fixed rough walls (obtained by randomly glued particles) at a constant volume fraction [37, 38]. The rectangular simulation box dimensions are $(L_x, L_y, L_z) = (25R, 10R, 27R)$, where L_z is the distance between the two walls and R the radius of the largest particle in the simulations. We use periodic boundary conditions in both x and y directions. The presence of hard confinement mimics experimental conditions, and simulations with Lee-Edwards boundary conditions that are periodic in the three directions show the same qualitative behavior (see Supplemental Material). The particle radii are uniformly distributed between $0.8R$ and R to prevent crystallization. When fixing ϕ , μ_0 , R , ρ_p and s_c , the physics of the system is characterized by a single dimensionless

number: $\lambda = \sqrt{\tau\rho}R/\eta_f$. λ can be understood as the ratio between the microscopic time scale of the lubricating fluid, η_f/τ , and of the granular medium, $R\sqrt{\rho/\tau}$ [24]. Increasing the shear stress τ quadratically is equivalent to decreasing η_f linearly. In our simulations, we vary η_f and keep τ fixed. After the system has reached its steady state with a linear velocity profile (no shear bands), we measure the time averaged velocity of the moving wall $\langle v_{wall} \rangle$, thus $\dot{\gamma} = \langle v_{wall} \rangle/L_z$ and the apparent viscosity of the suspension η is given by $\tau/\dot{\gamma}$. The quantities $\dot{\gamma}$, τ and η are measured in units of $\eta_f/\rho_p R^2$, $\eta_f^2/\rho_p R^2$ and η_f (see Supplemental Material for details).

The simulations (see Figs.1b and 2) reproduce a transition between a Newtonian regime at low shear rates (independent of μ_0 and dominated by HD-lubricated contacts) to a ST regime with increasing $\dot{\gamma}$, for which boundary lubricated contacts are dominating. In the absence of hydrodynamics in the friction law, such a transition is lost (see Supplemental Material). Indeed, in Fig.1c for increasing applied stress, the distributions of s in all the particle contacts shift toward the BL regime in the Stribeck curve. In our simulations, the system shear thickens when at least $\approx 20\%$ of the contacts are below s_c . In Fig.1d, the percentage of particles in BL and HD contacts is plotted against $\dot{\gamma}$ for the stresses defined in Fig.1b. For low μ_0 , this ST regime is continuous and fits with a Bagnoldian scaling ($\eta \propto \dot{\gamma}$). Here, the viscosity increases with μ_0 , as in a dry granular medium [24]. This scenario changes as μ_0 goes beyond a critical value, here 0.35 for $\phi = 0.58$ (Fig.2). Then, the system cannot be sheared above a critical shear rate for any shear stress: the system shear-thickens discontinuously.

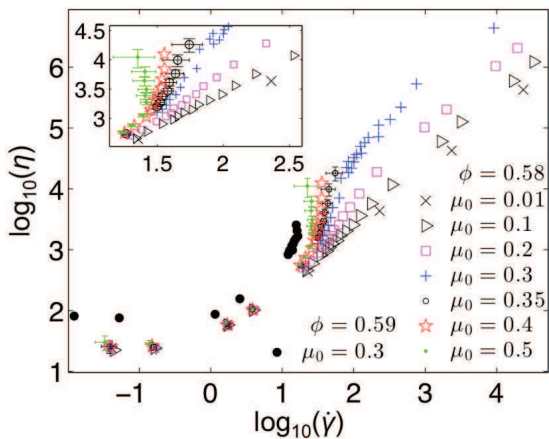


FIG. 2. (color online) Apparent viscosity versus $\dot{\gamma}$ for different μ_0 and $s_c = 5 \cdot 10^{-5}$ in simulations. In the Newtonian regime, the viscosity does not depend on μ_0 but on ϕ . At $\phi = 0.58$, for $\mu_0 \leq 0.3$, the system experiences CST, where the viscosity depends on the friction coefficient. For $\mu_0 \geq 0.35$, the system jams at sufficiently large $\dot{\gamma}$. Data points for $\phi = 0.59$ show DST for $\mu_0 = 0.3$. Inset: Zoom of the transition zone.

The transition from CST to DST does not only occur when increasing μ_0 but also when increasing ϕ : the system experiences CST at $\phi = 0.58$, $\mu_0 = 0.3$ but experiences DST for $\phi = 0.59$ and the same μ_0 (see Fig2). Moreover, as predicted in our theoretical model, the CST-DST transition occurs when ϕ is increased above a $\phi_{max}^{BL}(\mu_0=0.3)$, compatible with [28].

In brief, the numerical simulations confirm that our theoretical framework sets the sufficient conditions to explain Nw-ST and CST-DST transitions.

Our model is also independently supported by experiments where the link between local friction and macroscopic rheology is established using quartz surfaces. We first show experimentally that the volume fraction of the CST-DST transition is indeed ϕ_{max}^{BL} and then that it can be tuned by modifying μ_0 . This is demonstrated by using four different comb polymers, i.e. poly(methacrylic acid) (PMAA) grafted with poly(ethylene glycol) (PEG) side chains, which are dissolved in a $Ca(OH)_2$ saturated aqueous buffer solution with 20 mmol/L K_2SO_4 . The co-polymers were synthesized by radical polymerization in water according to [39, 40]. Their specifications, obtained from aqueous gel permeation chromatography (GPC) are (backbone size in kDa, number of carboxylic acids per side chain and side chain size in kDa): Polymer A: PMAA(4.3)-g(4)-PEG(2), Polymer B: PMAA(3.4)-g(2.3)-PEG(2), Polymer C: PMAA(4.3)-g(4)-PEG(0.5) and Polymer D: PMAA(5)-g(1.5)-PEG(2). Once in the buffer solution, these comb polymers are readily adsorbed onto a negatively charged surface, such as quartz, by calcium-ion bridging, and create a stable and highly solvated PEG coating on the solid surface [41] that is known to modify the BL coefficient of friction [42]. The conclusions of the experiments are not dependent on the choice of system, which is a model material for industrial applications (e.g. cement slurry), for which the friction coefficient can be easily tuned.

The rheological analysis was performed on suspensions of ground quartz (Silbelco France C400, $D_{50} = 12\mu m$) with Φ between 0.47 and 0.57 in the alkali polymer solutions (see Supplemental Material for details). We initially measured ϕ_{max}^{BL} via compressive rheology by high-speed centrifugation (acceleration $\approx 2000g$) of a fairly low concentration suspension ($\phi = 0.47$) in a 10mL measuring flask and calculating the average sediment volume fraction for the various polymers. During sedimentation at high speed, particles come into contact and jam, producing a looser sediment compared to frictionless objects. After 20 minutes of centrifugation, no further evolution is observed and we measured $\phi_{max}^{BL}(A) = 0.578$, $\phi_{max}^{BL}(B) = 0.560$, $\phi_{max}^{BL}(C) = 0.555$, $\phi_{max}^{BL}(D) = 0.545$ (see Fig.3a).

The CST-DST transition was then measured by shear

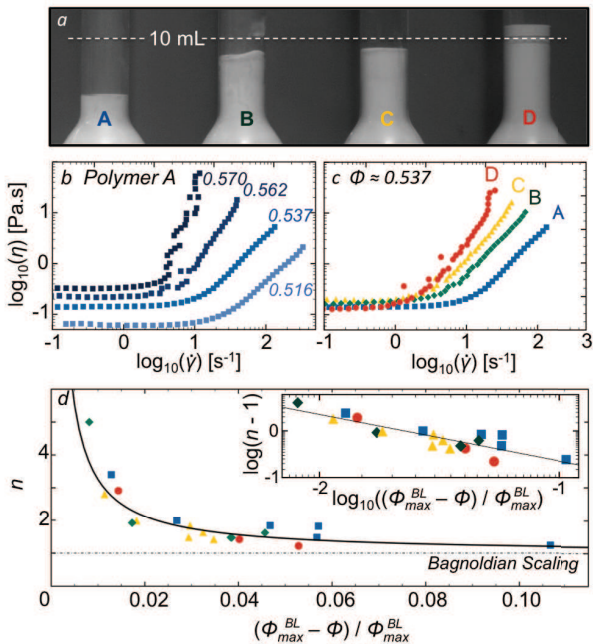


FIG. 3. (color online) a) Sediment heights for the different polymers after centrifugation. b) Viscosity vs shear rate with adsorbed polymer A for various ϕ of quartz microparticle suspensions. c) Viscosity vs shear rate for the four adsorbed polymers at analogous ϕ ($\phi(A) = 0.537$, $\phi(B) = 0.537$, $\phi(C) = 0.538$, $\phi(D) = 0.535$). d) Oswald-De Waele exponent n vs the reduced volume fraction (same symbols as in c). Inset: Same data in log-log plot. The solid line is a power-law fit for $(n - 1)$ vs reduced volume fraction.

rheometry in a helicoidal paddle geometry (Anton Paar 301 rheometer, see [21] Fig.4 for geometry description) with a descending logarithmic stress ramp after pre-shear (from 700 to 0.01 Pa in 100s). The viscosity curves are divided into two main parts: at low shear rate, the fluid shows a Newtonian behavior with a viscosity that depends on volume fraction [43] (Fig.3b) but not on the polymer coating (Fig.3c). For high shear rates, the fluid shear-thickens. At moderate volume fractions, the system undergoes CST with $\tau \propto \dot{\gamma}^2$ (Bagnoldian regime) as observed by [44], while for the higher volume fractions in our experiment, the abruptness of ST increases quickly at a critical Φ (see Fig.3b for Polymer A). Above this threshold, the suspensions display DST. In order to quantify this critical volume fraction, the flow curves for the various ϕ in the ST regime are fitted by an Oswald-De Waele power law: $\eta \propto \dot{\gamma}^n$. In Fig.3d, we show that $n(\phi)$ diverges exactly at the polymer-dependent ϕ_{max}^{BL} that we measured independently by centrifugation, as predicted by our model. Moreover, the data from the different polymer coatings collapse onto a single master curve as a function of a reduced volume fraction $(\phi_{max}^{BL} - \phi) / \phi_{max}^{BL}$ that does not depend on surface properties. A similar collapse was observed for particles of different shapes [45].

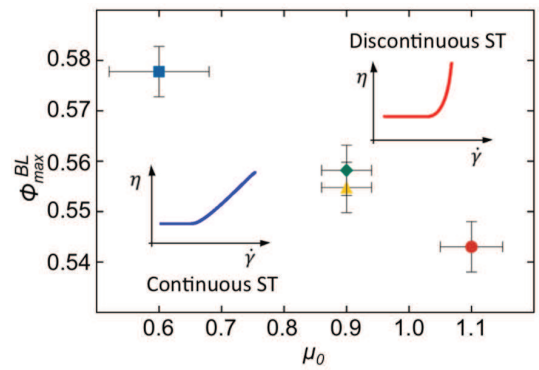


FIG. 4. (color online) ϕ_{max}^{BL} as a function of the coefficient of friction in boundary regime μ_0 for the four polymers (same symbols as in Fig.3). The CST and DST regions are highlighted in the graph.

To complete our analysis we measured the BL friction coefficients μ_0 between a polished rose quartz stone surface (Cristaux Suisses, Switzerland) and a 2 mm diameter borosilicate sphere (Sigma-Aldrich, USA) coated with the four different polymers, using a nanotribometer (CSM instruments, Switzerland). The contact was immersed into a drop of polymer solution. The experiments were realized in an N_2 atmosphere at sliding velocities between 10^{-5} and 10^{-3} m/s (see Supplemental Material for a protocol). The measured values of μ_0 reported Fig.4in are speed independent, as expected in the BL regime. The differences in the friction for the different polymers have been previously ascribed to a variation of the PEG unit density on the surfaces [46], stemming from an equilibrium between entropic side chain repulsion and backbone/surface electrostatic attraction (through calcium bridging).

Finally, Fig.4 shows the direct correlation between the BL coefficients of friction and the measured maximum volume fraction ϕ_{max}^{BL} that separates CST and DST, as included in our model. ϕ_{max}^{BL} is a decreasing function of the particle friction coefficient in the boundary regime, as predicted by simulations [28, 29].

Using a simple theoretical framework, independently backed up by simulations and experiments, we have identified the microscopic origin of both continuous and discontinuous shear-thickening of dense non-Brownian suspensions as the consequence of the transition from hydrodynamically lubricated to boundary lubricated contacts. The central role played by friction introduces the local Sommerfeld number as the controlling parameter for the transition between Newtonian and shear-thickening regimes, as demonstrated by our numerical simulations. The presence of two distinct lubrication regimes as a function of the Sommerfeld number is furthermore at the origin of the Nw-ST transition. In particular, the friction coefficient in the boundary regime, which we tuned ex-

perimentally by polymer adsorption on the particle surface, governs the nature of the ST transition. Distinct lubrication regimes imply that the jamming volume fractions in the viscous regime ϕ_{max}^{HD} and in the Bagnoldian regime ϕ_{max}^{BL} are not the same in general, given that only the latter depends on the friction coefficient. Therefore CST is found when $\phi_{max}^{HD} \geq \phi_{max}^{BL} \geq \phi$, while the suspension exhibits DST when the transition to the inertial regime is impossible because $\phi_{max}^{HD} \geq \phi > \phi_{max}^{BL}$. Thus, in the absence of transient migration effects [44], the local volume fraction and friction coefficient determine the stable microscopic flow mechanism, which is either CST or DST [44, 47, 48]. Moreover, our model does not require any confinement at the boundaries, but only that locally $\phi > \phi_{max}^{BL}$. This condition is fulfilled by preventing particle migration out of the shear zone, either by confinement during steady-state shear [18] or by keeping the shear duration short enough [49].

The generality and consistency of our data and of the proposed model sets a global framework in which the tribological (friction) and rheological properties of dense non-colloidal systems are intimately connected. This concept is expected to have an impact on a host of practical applications and relates fundamental issues such as flow localization [50] and the solid-liquid-solid transition of granular pastes [14].

Acknowledgments - The authors thank Fabrice TOUSSAINT for scientific discussions during preliminary work and Cédric JUGE, Abdelaziz LABYAD and Serge GHILARDI for technical support.

The authors acknowledge financial support by Lafarge LCR. Furthermore, this work was supported by the FP7-319968 grant of the European Research Council, the Ambizione grant PZ00P2_142532/1 of the Swiss National Science Foundation and the HE 2732/11-1 grant of the German Research Foundation.

* Corresponding author: lucio.isa@mat.ethz.ch

- [1] R. Larson, *The structure and rheology of complex fluids* (Oxford University, 1999).
- [2] P. Coussot and C. Ancey, *Rhéophysique des pâtes et des suspensions* (EDP Sciences, 1999).
- [3] H. Barnes, *Journal of Rheology* , 329 (1989).
- [4] E. Andrade and J. Fox, *Proceedings of the Physical Society. Section B* , 483 (1949).
- [5] R. A. Bagnold, *Proceedings of the Royal Society A: Mathematical, Physical and Engineering Sciences* **225**, 49 (1954).
- [6] J. F. Brady and G. Bossis, *Journal of Fluid Mechanics* **155**, 105 (1985).
- [7] R. Hoffman, *Transactions of the Society of Rheology* **16**, 155 (1972).
- [8] W. Boersma, J. Laven, and H. N. Stein, *AICHE Journal* **36**, 321 (1990).
- [9] N. J. Wagner and J. Brady, *Physics Today* , 27 (2009).
- [10] J. Bergholtz, J. F. Brady, and M. Vucic, *Journal of Fluid Mechanics* **456**, 239 (2002).
- [11] X. Cheng, J. H. McCoy, J. N. Israelachvili, and I. Cohen, *Science* **333**, 1276 (2011).
- [12] M. Cates, J. Wittmer, J. Bouchaud, and P. Claudin, *Physical Review Letters* **81**, 1841 (1998).
- [13] J. Morris, *Rheologica Acta* **48(8)**, 909 (2009).
- [14] A. Fall, N. Huang, F. Bertrand, G. Ovarlez, and D. Bonn, *Physical Review Letters* **100** (2008).
- [15] L. Isa, R. Besseling, A. Morozov, and W. Poon, *Physical Review Letters* **102** (2009), 10.1103/PhysRevLett.102.058302.
- [16] E. Brown and H. Jaeger, *Physical Review Letters* **103** (2009).
- [17] E. Brown, N. A. Forman, C. S. Orellana, H. Zhang, B. W. Maynor, D. E. Betts, J. M. DeSimone, and H. M. Jaeger, *Nature Materials* **9**, 220 (2010).
- [18] E. Brown and H. Jaeger, *Arxiv preprint* (2010).
- [19] P. Coussot and N. J. Wagner, *Rheologica Acta* **48**, 827 (2009).
- [20] D. Lootens, H. Van Damme, Y. Hémar, and P. Hebraud, *Physical Review Letters* **95** (2005).
- [21] F. Toussaint, C. Roy, and P. H. Jézéquel, *Rheologica Acta* **48**, 883 (2009).
- [22] H. Lombois-Burger, P. Colombet, J. Halary, and H. Van Damme, *Cement and Concrete Research* **38**, 1306 (2008).
- [23] G. W. Stachowiak and A. W. Batchelor, *Engineering tribology* (Butterworth-Heinemann, 2005).
- [24] Y. Forterre and O. Pouliquen, *Annual Review of Fluid Mechanics* , 1 (2008).
- [25] M. Trulsson, B. Andreotti, and P. Claudin, *Physical Review Letters* **109-11**, 118305.
- [26] F. Boyer, É. Guazzelli, and O. Pouliquen, *Physical Review Letters* **107**, 188301 (2011).
- [27] N. Roussel, A. Lemaître, R. Flatt, and P. Coussot, *Cement and Concrete Research* **40** (2010).
- [28] L. E. Silbert, *Soft Matter* **6**, 2918 (2010).
- [29] M. P. Ciamarra, R. Pastore, M. Nicodemi, and A. Coniglio, *Physical Review E* **84** (2011), 10.1103/PhysRevE.84.041308.
- [30] N. A. Frankel and A. Acrivos, *Chemical Engineering Science* **22**, 847 (1967).
- [31] J. J. Moreau, *European Journal of Mechanics: Part A Solids* **13**, 93 (1994).
- [32] M. Jean and J. J. Moreau, *Contact Mechanics International Symposium* , 31 (1992).
- [33] L. Brendel, T. Unger, and D. E. Wolf, *The Physics of Granular Media* (Wiley-VCH, 2004).
- [34] R. Mani, D. Kadau, D. Or, and H. J. Herrmann, *Physical Review Letters* **109**, 248001 (2012).
- [35] D. Kadau, J. Andrade Jr., and H. Herrmann, *The European Physical Journal E* **30**, 275 (2009).
- [36] D. Barthes-Biesel, *Microhydrodynamics and Complex Fluids* (CRC Press, 2012).
- [37] M. Ltzell, S. Luding, H. Herrmann, D. Howell, and R. Behringer, *The European Physical Journal E* **11**, 325 (2003).
- [38] A. Pea, P. Lind, S. McNamara, and H. Herrmann, *Acta Mechanica* **205**, 171 (2009).
- [39] D. Rinaldi, T. Hamaide, C. Graillat, F. D'Agosto, R. Spitz, S. Georges, M. Mosquet, and P. Maitresse, *Journal of Polymer Science Part A: Polymer Chemistry* **47**, 3045 (2009).

- [40] J. A. Jones, N. Novo, K. Flagler, C. D. Pagnucco, S. Carew, C. Cheong, X. Z. Kong, N. A. D. Burke, and H. D. H. Stöver, *Journal of Polymer Science Part A: Polymer Chemistry* **43**, 6095 (2005).
- [41] R. J. Flatt, I. Schober, E. Raphael, C. Plassard, and E. Lesniewska, *Langmuir* **25**, 845 (2009).
- [42] S. Lee and N. D. Spencer, *Science* **319**, 575 (2008).
- [43] I. M. Krieger and T. J. Dougherty, *Transactions of the Society of Rheology* **3**, 137 (1959).
- [44] A. Fall, A. Lemaitre, F. Bertrand, D. Bonn, and G. Ovarlez, *Physical Review Letters* **105** (2010), 10.1063/1.465782.
- [45] E. Brown, H. Zhang, N. A. Forman, B. W. Maynor, D. E. Betts, J. M. DeSimone, and H. M. Jaeger, *Physical Review E* **84** (2011).
- [46] S. S. Perry, X. Yan, F. T. Limpoco, S. Lee, M. Müller, and N. D. Spencer, *ACS Applied Materials & Interfaces* **1**, 1224 (2009).
- [47] A. Fall, PhD thesis, Université Paris VII (2008).
- [48] A. Fall, F. Bertrand, G. Ovarlez, and D. Bonn, *Journal Of Rheology* **56**, 575 (2012).
- [49] S. R. Waitukaitis and H. M. Jaeger, *Nature* **487**, 205 (2012).
- [50] N. Huang, G. Ovarlez, F. Bertrand, and S. Rodts, *Physical Review Letters* **94** (2005).